Title

Compensation strategy for constructing high-performance aerogels using acrylamide-assisted vacuum drying and their use as water-induced electrical generators

Authors

Fan, Juncheng
Li, Hengrui
Tang, Songsong
et al.

Publication Date

2023

DOI

10.1016/j.cej.2022.139685

Peer reviewed

Chemical Engineering Journal 452 (2023) 139685

Contents lists available at ScienceDirect

Chemical Engineering Journal

journal homepage: www.elsevier.com/locate/cej

Compensation strategy for constructing high-performance aerogels using acrylamide-assisted vacuum drying and their use as water-induced electrical generators

Juncheng Fan [a], Hengrui Li [a], Songsong Tang [a], Boxiao Li [a], Yangyang Xin [b], You-Lo Hsieh [c], Jian Zhou [a,*]

[a] School of Material Science and Engineering, Key Laboratory for Polymeric Composite, Functional Materials of Ministry of Education, State Key Laboratory for Optoelectronic Materials and Technologies, Guangzhou Key Laboratory of Flexible Electronic Materials and Wearable Devices, Sun Yat-sen University, Guangzhou, Guangdong 510275, China

[b] School of Materials Science and Engineering, Nanyang Technological University, 50 Nanyang Avenue, 639798 Singapore, Singapore

[c] Biological and Agricultural Engineering, Chemical Engineering, University of California at Davis, Davis, CA 95616-8722, United States

ARTICLE INFO

Keywords:
PEDOT/PSS
Aerogel
Acrylamide
Sublimation
Vacuum drying

ABSTRACT

Developing novel, energy-saving, and facile approaches to constructing high-performance aerogels is still challenging. Aerogels are most commonly produced by freeze-drying and supercritical drying that require expensive specialty equipment or ambient drying lengthily of solvent exchange precursors. Here, we report a compensation strategy using acrylamide as an assisting solute to enable the construction of conductive polymer aerogels by simple vacuum drying of frozen solids of aqueous poly(3,4-ethylene dioxythiophene)/poly(styrene sulfonate) (PEDOT/PSS). In this approach, the acrylamide crystal sublimates slowly at an elevated temperature (80 or 110 °C) to maintain the porous structure of PEDOT/PSS in the solid-state during water evaporation. By tuning PEDOT/PSS to acrylamide weight ratios and drying temperatures, aerogels were produced with low density (6.3–21.6 mg/cm^3), high porosity (>99 %), and low shrinkage (5.3 %). Additionally, acrylamide increases the electrical conductivity of PEDOT/PSS by three orders of magnitude (from 0.01 to 81.1 S/m). Morphology and physical properties are further analyzed to reveal aerogel formation and the conductivity enhancement mechanism. These aerogels are then applied as water-induced electric generators for green energy harvesting. The current work provides an alternative and simplified approach to rapidly fabricating various nanomaterial-based aerogels, replacing the slower and more expensive freeze-drying and supercritical drying.

1. Introduction

Aerogels are ultra-high porous three-dimensional (3D) structures comprising up to 99.98 % air, supported by either cellular or fibrous network as the skeleton [1–4]. Their excellent physical properties like ultra-low density, high surface area, low thermal conductivity, low acoustic impedance, and so on have shown great potential in energy storage, chemical catalysts, electronic sensors, acoustic insulators, aerospace, and thermal insulators [5–11].

Though with brilliant promises for advanced applications, aerogels' scalability and industrial preparation still face tremendous obstacles. Aerogels have been most commonly prepared by either supercritical drying of precursor gels in the supercritical state or freeze-drying from a frozen state to avoid the effect of high surface tension and capillary pressure of the liquid phase [2–9,12–15]. Both drying approaches rely on specialized instruments, such as supercritical-drier or lyophilizer, and are energy and time-consuming. Ambient drying uses none of the expensive and potentially dangerous high-pressure equipment but requires multiple and complex processing steps like solvent thawing and exchange, thus is limited and non-universal [16–19]. For instance, graphene aerogels have been constructed from ambient drying by sublimation of gel frozen in an organic solvent with a higher boiling temperature and vapor pressure [18]. Aerogels with a density of 23–38 mg/cm^3 were obtained by ambient drying of cellulose nanofibers (CNFs) and alginate, but exhibiting considerable shrinkage (25–60 %) due to the weaker coordination between the carboxyl group and the divalent ion

* Corresponding author.
E-mail address: zhouj296@mail.sysu.edu.cn (J. Zhou).

https://doi.org/10.1016/j.cej.2022.139685
Received 28 July 2022; Received in revised form 23 September 2022; Accepted 5 October 2022
Available online 8 October 2022

[17]. We have demonstrated crosslinking CNFs and carboxymethylated chitosan using a triazine derivative allowed ambient drying for the structural design of aerogels with a low density of 12 mg/cm^3 and a low shrinkage (10 %) [16]. Although the crosslinked structure could withstand the surface tension and capillary pressure of the liquids during evaporation, a large amount of organic solvent (ethanol and acetone) was needed for thawing and solvent exchange processes [16–19].

Therefore, the main goal of this study is to construct aerogels without using typical lyophilizers, supercritical dryers, or ambient drying that consumes large amounts of organic solvents (solvent thawing and

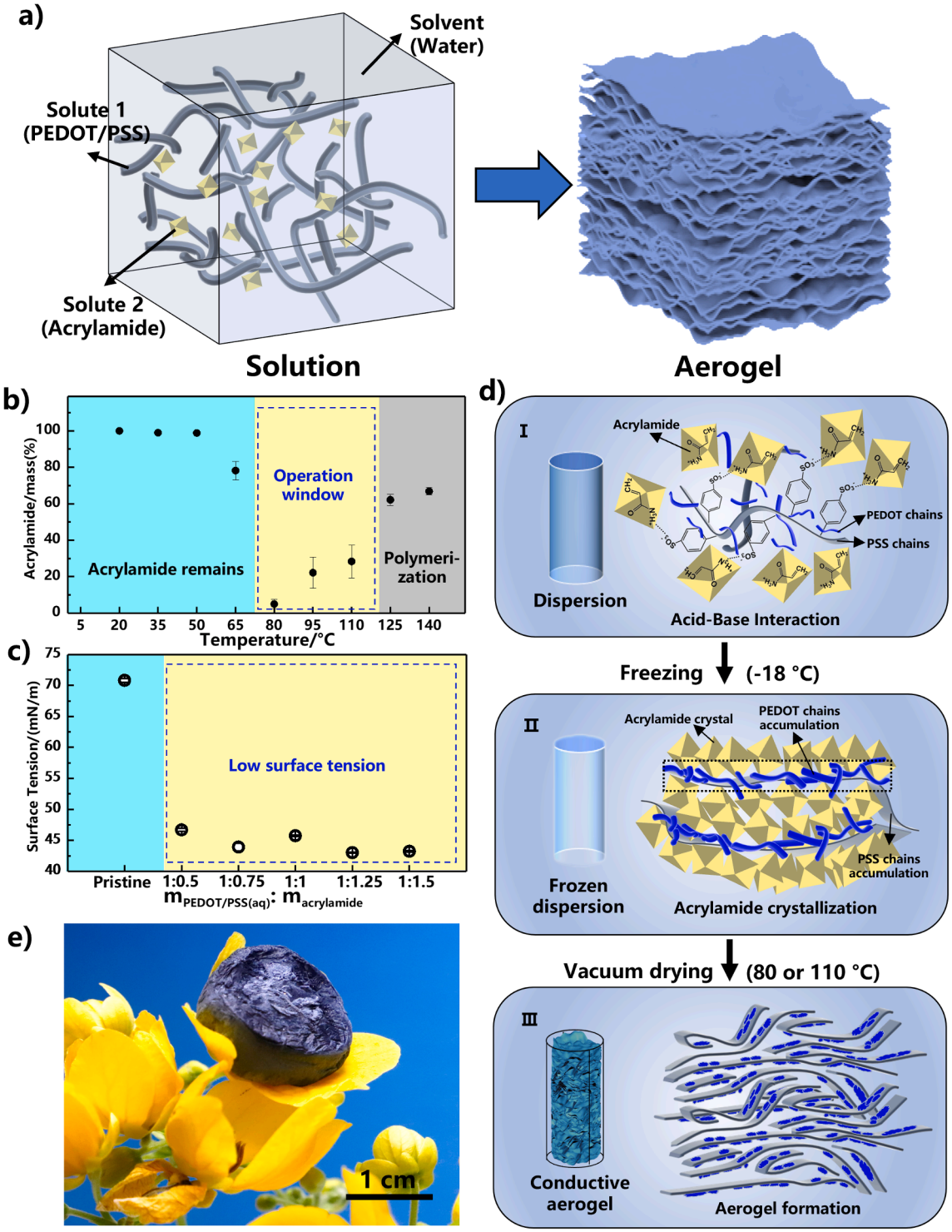

Fig. 1. Proposed aerogel formation principle using acrylamide-assisted vacuum drying. a) A new concept for aerogel formation. Solute 1 is the target material, and solute 2 is the assistant material for aerogel formation. b) Feasible temperature operation window of the acrylamide for aerogel formation. c) The surface tension of PEDOT/PSS aqueous dispersion dramatically reduced after adding acrylamide. d) Schematic of the procedure to prepare the PEDOT/PSS aerogel. (I) The sulfonic acid groups from PSS connect the acrylamide's amine groups through acid-base interaction. (II) The freezing process prompts the forming of the acrylamide crystal and leads to accumulation of the PEDOT and PSS chains, respectively. (III) After the vacuum drying process, the acrylamide crystal is removed, and the PEDOT/PSS aerogel remains. e) Photograph of acrylamide-assisted vacuum drying PEDOT/PSS aerogel on flowers.

exchange). Our concept is to use a compensation strategy that creates a system containing two solutes in the aqueous dispersion (Fig. 1**a**). Solute 1 is the target material for the cellular network, and solute 2 is the assistant material that serves as a solid skeleton to support the gel of solute 1 during solvent removal. Based on this hypothesis, solute 2 must withstand the surface tension and capillary pressure during the solvent removal process and subsequently eliminate itself to compensate for solute 1. In this study, a conductive polymer, poly(3,4-ethylene dioxythiophene)/poly(styrene sulfonate) (PEDOT/PSS), is first conducted as the target material as it has been widely exploited in thermoelectric devices, tissue engineering, polymer solar cells, sensors, and flexible electronics [20–24]. Acrylamide is selected as solute 2 and the supporting material during vacuum drying.

Herein, we successfully demonstrated the construction of PEDOT/PSS aerogel employing acrylamide to enable simple vacuum drying, overcoming the need for specialty instruments and multi-step preparation. Due to the acid-base interactions between acrylamide and PSS and the polar effect of acrylamide on PEDOT, acrylamide crystals herein function similarly to the ice crystals in freeze-drying in creating the porous structure [2,25,26]. Acrylamide serves to reduce surface tension, thus capillary pressure to retain the porous network and reduce shrinkage. Meanwhile, acrylamide facilitates the transformation of the PEDOT structure from benzoid-rich to quinoid-rich phase, improving conductivity. Aerogels were also similarly prepared with other biopolymers and nano-materials to investigate the universality of the acrylamide-assisted vacuum drying approach. Then the potential application of these aerogels in the water-induced electric generator is conducted. The compensation strategy of acrylamide-assisted vacuum drying proposes an alternative for developing customized aerogels and stimulates their applications in energy generation.

2. Result and discussion

2.1. Formation principle of the aerogel

Here, aqueous PEDOT/PSS dispersion is the starting material, in which PEDOT/PSS is solute 1 in the solvent, i.e., water. Our strategy is to construct the aerogel via vacuum drying under reduced pressure and remove the ice crystals in the frozen PEDOT/PSS aqueous dispersion. Thus, the essential role of solute 2 must serve as a skeleton and favor the high-temperature ublimation process. Acrylamide is a reactive monomer and intermediate in synthesizing polymers and producing organic chemicals [27,28]. Acrylamide, a white crystalline solid, has a 0.67 Pa vapor pressure at 25 °C (vapor saturation method), melts at 84.5 °C, polymerizes rapidly at elevated temperatures, and boils at 125 °C at 3.33 kPa [29–31]. The higher boiling point of acrylamide than water at relatively low vapor pressure makes it a candidate for solute 2.

As sublimation of any compound depends on temperature and pressure [32,33], the extent of sublimation of acrylamide at varied temperatures under vacuum was profiled to determine the feasible temperature window for aerogel formation (Fig. 1**b**). Acrylamide was dried in a vacuum oven at 20 to 140 °C for 6 h. Acrylamide remains solid in regime I (T < 50 °C) due to little sublimation. In regime III (T > 110 °C), acrylamide polymerizes easily into poly-acrylamide, gaining polymer to give 62 % and 67 % mass at 125 °C and 140 °C, respectively. Under the continuous vacuum drying at elevated temperature, acrylamide mass was reduced to as low as 5 % at 80 °C, and 25 % and 28 % at the higher 95 °C and 110 °C, indicating optimal sublimation. Thus, we chose regime II (65 °C ≤ T ≤ 110 °C) as the possible operation window for preparing the aerogels, and three different temperatures of 50, 80, and 110 °C were investigated to confirm the acrylamide-assisted vacuum drying approach for aerogel formation.

Moreover, five different PEDOT/PSS (aq)-to-acrylamide weight ratios (1:x, x = 0.5, 0.75, 1, 1.25, 1.5) were used to investigate acrylamide's role and to optimize the aerogel formation process (**Table S1**, see details in experiment section). Fig. 1**c** shows that acrylamide reduced the surface tension, γ, of aqueous PEDOT/PSS dispersion sharply from 70.3 to around 44.5 mN/m, irrespective of their weight ratios. The decrease is attributed to the significant quantities of acrylamide with hydrophobic–$CH=CH_2$ and hydrophilic–$CONH_2$, serving as a surfactant for the PEDOT/PSS complex [34]. This low surface tension is critical to reduce the capillary pressure or pull on the PEDOT/PSS structure during removing the liquid solvent from the wet gel matrix. The Young-Laplace equation is used to calculate the capillary pressure P, and the micropores in aerogel are modeled as cylinders [13].

$$P = \frac{2\gamma cos\theta}{R}$$

where θ is the contact angle between the solvent and contacting surface, and R is the diameter of the micropores in the drying process. Accordingly, as the γ decreases with the introduction acrylamide in PEDOT/PSS aqueous dispersion (Fig. 1**c**), the capillary pressure P decreases to lower the pull to prevent the PEDOT/PSS structure from collapsing as the solvent is removed. In control, thin nanostructures of an unmodified wet PEDOT/PSS gel are easily destroyed by the surface tension as the interface of liquid and vapor retreats and capillary pressure causes the fracture to the aerogel [12,15]. With acrylamide the considerably lowered surface tension and thus capillary pressure helps to preserve the aerogel structure in the drying process.

Fig. 1**d** illustrates the aerogel formation procedure and proposed mechanism. First, the PEDOT/PSS aqueous dispersion (pH = 2.1) is mixed with acrylamide. The acid-base interaction between the primary amine of acrylamide and the sulfonic group of PSS occurs (Fig. 1**d-I**), possibly leading to phase separation of PEDOT and PSS. After freezing at −18 °C for 12 h, the nucleation and crystallization of water and acrylamide gradually extrude the PEDOT/PSS to form the 3D structure (Fig. 1**d-II**). Subsequently, acrylamide interacts with the PSS through ionic bonding during the crystallization, probably leading to aggregation of the separated PEDOT at the edge of the crystal. This process may result in phase separation of PEDOT and PSS.

The porous structure can be retained after vacuum drying, mainly due to the slower sublimation of acrylamide crystals **(**Fig. 1**d-III)**. The acrylamide crystal sublimates much slower than water evaporation and maintains a solid-state to support the overall structure inside aerogels. Further sublimation without capillary pressure continues until the acrylamide removes completely and the cellular structure remains. Substantial acrylamide crystals, serving as a supporting framework, prevent the PEDOT/PSS wet gel infrastructure from collapsing during ice/solvent removal. This process is similar to freeze-drying, which removes the ice crystal in sublimation under extremely low temperatures (-50 °C) and pressure [25,26].

As suggested in Fig. 1**a**, the ice and acrylamide crystal is exposed to a high temperature in a vacuum. During the drying stage, two main processes are involved, the water's evaporation and the sublimation of acrylamide. The water is removed by evaporation after the thawing of ice. The ice crystal quickly melts and evaporates before the surface tension and capillary pressure cause widespread collapse of the porous structure. The acrylamide crystal sublimates much slower and maintains a solid state to support the overall porous structure in the aerogels. After continuous vacuum drying for 6 h, an aerogel cake with 12.5 cm^2 × 0.8 cm is prepared through the above-mentioned novel approach. It presents a density of 20.2 mg/cm^3, and Cassia surattensis Burm flowers can support it without deforming their structures (Fig. 1**e**). In contrast, the frozen PEDOT/PSS dispersion without acrylamide melts and collapses (**Fig. S1**). Using the same method, aerogels with different densities (6.3–21.6 mg/cm^3) are fabricated simply by changing the ratio of PEDOT/PSS dispersion and acrylamide loading. Moreover, this approach also presents a possible cyclic utilization of acrylamide (Fig. S2**a**). In the vacuum oven, the glass door whose temperature is lowered by the ambient temperature spontaneously collects the crystallized acrylamide (Fig. S2**c**). This recycled acrylamide from the glass can be reused to prepare additional PEDOT/PSS aerogel by the

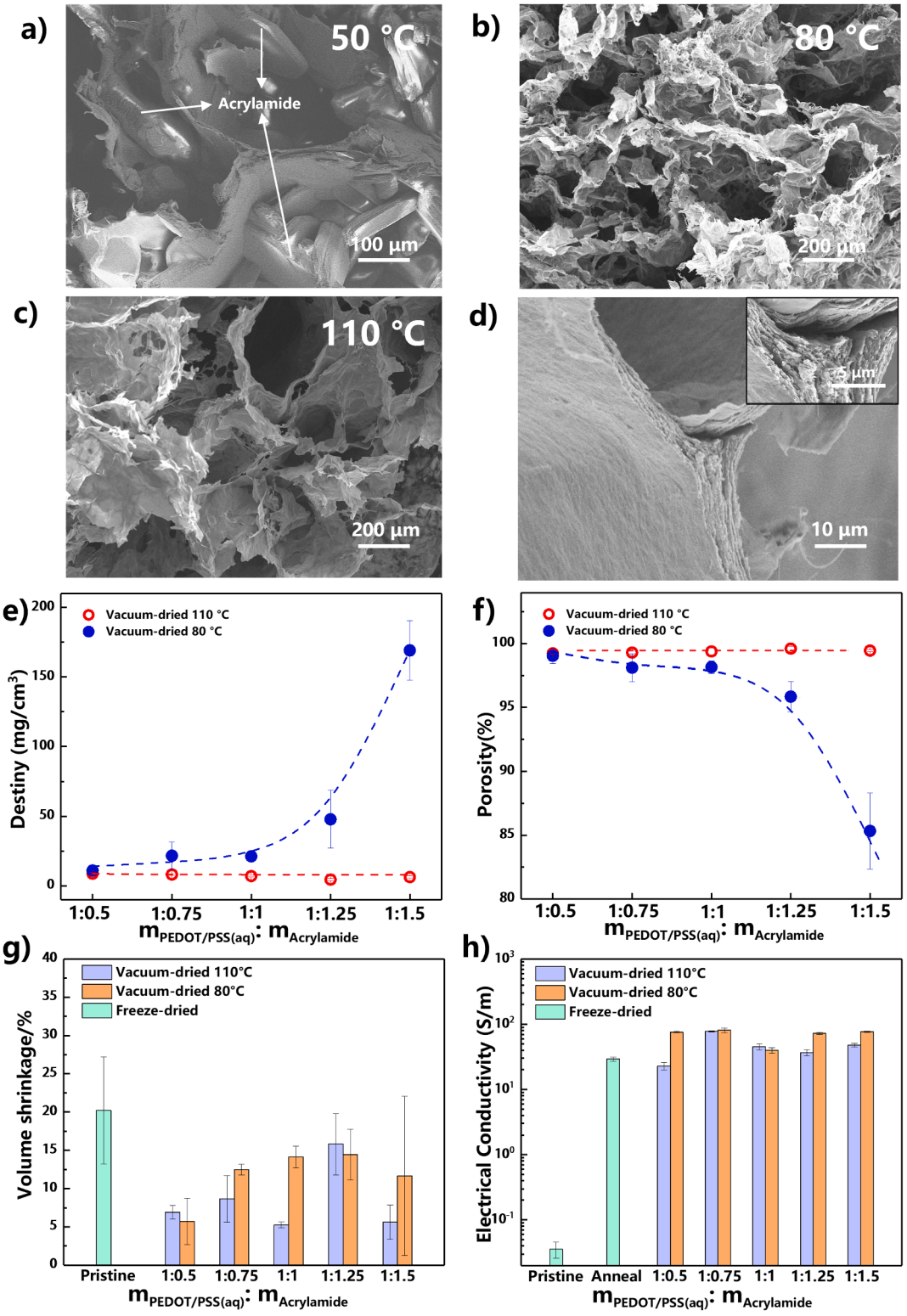

Fig. 2. Morphology and physical properties of the conductive polymer aerogels. a) The SEM image of the sample was obtained after vacuum drying at 50 °C. The solid pieces of crystal with a charging effect indicate the remaining acrylamide. b) and c) The SEM images of the aerogel obtained after vacuum drying at 80 °C and 110 °C, respectively, show highly porous structures. d) The aerogel displays the lamina structure due to the assistance of the acrylamide crystal. The insert image shows the stacking lamina on the edge of the micropores. e) The densities of different PEDOT/PSS aerogels prepared with the different weight ratios of PEDOT/PSS aqueous dispersion and acrylamide at 80 °C and 110 °C. The aerogel density prepared by vacuum drying at 110 °C is about 6.3 mg/cm^3. f) The porosity of PEDOT/PSS aerogels prepared with the different weight ratios of PEDOT/PSS (aq) and acrylamide at 80 °C and 110 °C. g) The freeze-dried and vacuum-dried PEDOT/PSS aerogel volume shrinkage. h) The electrical conductivity of PEDOT/PSS aerogels as a function of PEDOT/PSS aqueous dispersion to acrylamide weight ratios. The conductivity of vacuum-dried aerogels is three orders of magnitude improvement of the freeze-dried aerogel.

acrylamide-assisted vacuum drying approach (Fig. S2**d**, **Table S2**).

2.2. Morphology and physical properties of the conductive polymer aerogels

The microstructure of the materials vacuum-dried at different temperatures showed their morphology to be strongly temperature-dependent (Fig. 2). Despite 50 °C is not included in the operation windows, a sample prepared at 50 °C helps to understand the aerogel formation process and the working mechanism of the acrylamide. Drying at 50 °C did not create aerogels because it failed to remove the acrylamide crystal. Fig. 2**a** shows acrylamide crystals around the PEDOT/PSS cellular structures, displaying a charging effect under SEM due to their non-conductive nature. Moreover, the excluded lamellar PEDOT/PSS is observed in the cross-section. The solid pieces regularly align in the flank, indicating that the acrylamide crystal supports the PEDOT/PSS structure layer-by-layer (Fig. S3**a**). When the temperature increases to 80 °C and 110 °C (Fig. 2**b and 2c**), cellular structures are observed with pores ranging from tens to hundreds of micrometers, as shown in Fig. S4**a**. Further enlargements of the cellular walls show many layers of lamellar morphology (Fig. 2**d**) from both ice and acrylamide crystals. These PEDOT/PSS cellular walls hold up the micro and mesoporous layers by layers, corresponding to the formation structure of the acrylamide crystal layers (**Fig. S3**).

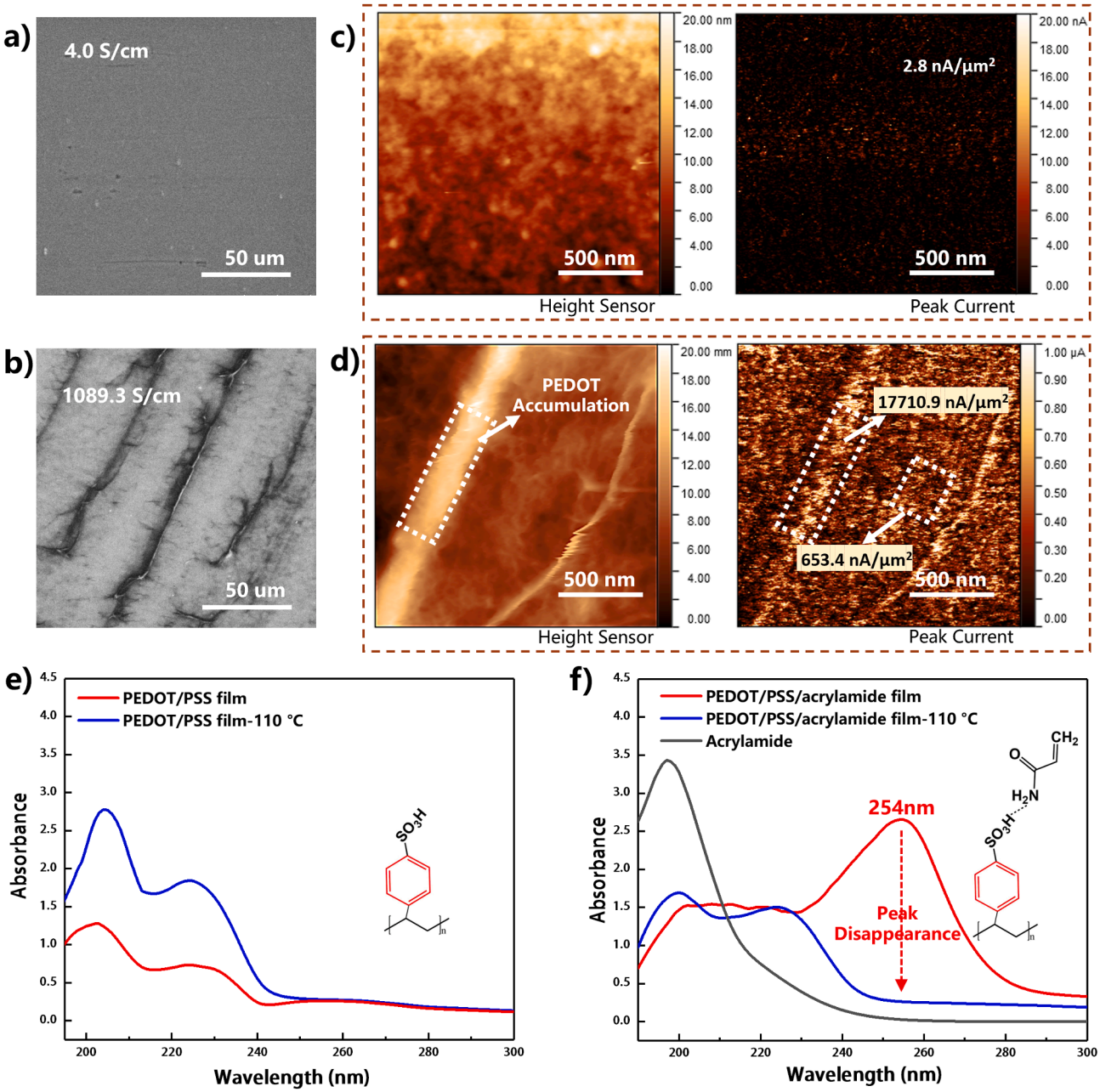

Fig. 3. Electrical conductivity enhancement mechanism in PEDOT/PSS using acrylamide. a) The SEM image of pristine spin-coated PEDOT/PSS film after vacuum drying. b) The SEM image of spin-coated PEDOT/PSS/acrylamide film after vacuum drying. c) Atomic force microscopy (AFM) height images of PEDOT/PSS film (after vacuum drying) and its corresponding current map. The mean current density of this area is 2.8nA/μm^2. d) AFM height images of the PEDOT/PSS/acrylamide film (after vacuum drying) and its corresponding current map. The bulging lines are strongly related to the higher mean current density (17710.9nA/μm^2). e) The UV–vis curve of the pristine film of PEDOT/PSS before and after vacuum drying. f) The UV–vis curve of acrylamide, the PEDOT/PSS/acrylamide film before and after vacuum drying.

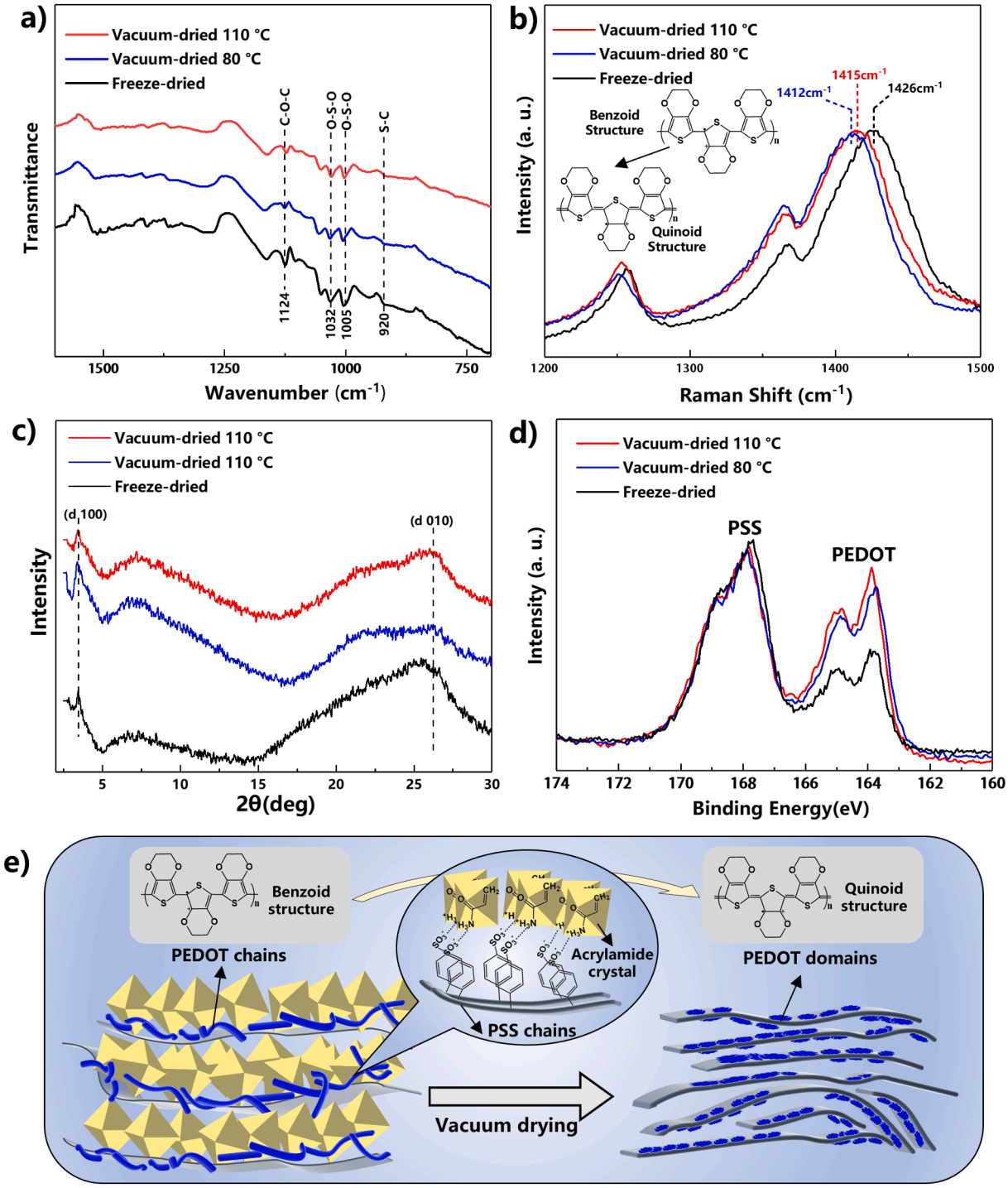

Fig. 4. Chemical and structural analysis of PEDOT/PSS aerogels. a) The FTIR transmittance of the freeze-dried and the vacuum-dried PEDOT/PSS aerogels at 110 and 80 °C. b) Raman spectrum of the freeze-dried and the vacuum-dried PEDOT/PSS aerogels at 110 and 80 °C. c) The X-ray diffractograms of the freeze-dried and the vacuum-dried PEDOT/PSS aerogels at 110 and 80 °C. d) XPS spectrum of the freeze-dried and the vacuum-dried PEDOT/PSS aerogels at 110 and 80 °C. The XPS intensity of PEDOT relative to PSS increases significantly resulting in higher conductivity. e) The confirmed formation mechanism of PEDOT/PSS aerogels shows that acrylamide is a supporting skeleton and conductivity enhancer during vacuum drying.

The incremental cyclic compression tests (strain = 20 %, 40 %, and 60 %) in the axial direction of the aerogels are conducted to compare their mechanical performances (Fig. S4**b-d**). To compare rationally, the freeze-dried solution is fixed with the same weight ratio of water instead of the acrylamide to ensure the same PEDOT/PSS content (Table S1). In these compression tests, the aerogels are all prepared with a ratio of 1:0.75. Fig. S4**b-d** shows that the aerogels cannot fully recover after each compressing. Moreover, after the cyclic compression at 60 % strain, they presented residual strains of about 42–50 % for the three samples. Their compressive stress at 60 % strain of freeze-dried aerogel, vacuum-dried aerogel at 110 °C, and vacuum-dried aerogel at 80 °C is 4.1, 3.5, and 3.6 kPa, respectively. The compressive modulus calculated from the last compression cycle of freeze-dried aerogel, vacuum-dried aerogel at 110 °C, and vacuum-dried aerogel at 80 °C is 6.07 kPa, 16.5 kPa, and 13.6 kPa, respectively. Comparing their envelope areas of corresponding curves at each incremental cycle, the area for vacuum-dried aerogel is

larger than that of freeze-dried aerogel, with an area ratio of about 1 to 0.8. The decrease in the modulus of the vacuum-dried aerogels in the last cycle also indicates the development of degradation while increasing the strain. These results suggest that more energy is needed to withstand the resistance of cellular structures in compressing the vacuum-dried aerogels.

Fig. 2**e** presents the density evolution of the aerogels with different weight ratios of PEDOT/PSS to acrylamide. The vacuum-dried PEDOT/PSS aerogels prepared at 80 °C show a low density of 21.2 mg/cm^3 when the PEDOT/PSS to acrylamide weight ratio is below 1:1. The higher proportion of acrylamide (weight ratio $>$ 0.75) increases density because the more acrylamide residual remains at 80 °C and a free-acrylamide aerogel could be obtained by increasing the heating time by$>$6 h. Other than that, raising the vacuum-dried temperature is another choice. Aerogels with a 6.3 mg/cm^3 density can be obtained at 110 °C when the PEDOT/PSS to acrylamide weight ratio is 1:1.25. This is ascribed to the improved efficiency of sublimation at higher temperatures. However, higher temperatures might lead to the polymerization of acrylamide, and it seems to become uncontrollable at a temperature above 110 °C where only a solid mixed with polyacrylamide and PEDOT/PSS is obtained. Instructed by the density measurement, the optimum PEDOT/PSS dispersion to acrylamide weight ratio is between 1:0.5–1:1.5 at 110 °C and below 1:0.75 at 80 °C. Fig. 2**f** shows the evolution of PEDOT/PSS aerogel porosity with the weight ratio of PEDOT/PSS (aq) and acrylamide. High porosity (up to 99 %) is obtained when the aerogels are vacuum-dried at 110 °C. However, the aerogels vacuum dried at 80 °C have lower porosities when the PEDOT/PSS (aq) to acrylamide weight ratio is higher than 1:1. The extent of remaining acrylamide inside the aerogel also increases density and lowers porosities of the aerogels. To compare the density and porosity of the freeze-dried aerogels rationally, the freeze-dried solution is fixed with the same weight ratio of water instead of the acrylamide to ensure the same PEDOT/PSS content (**Table S1**). As for freeze-dried aerogels, in Fig. S4**e**, they present a density of around 10 mg/cm^3 and porosity of around 99 %, similar to the result of the vacuum-dried aerogel at 110 °C. It indicates that vacuum drying is a reasonable alternative to freeze-drying. Moreover, the freeze-dried aerogel presents 20 % of volume shrinkage, obviously higher than vacuum-dried aerogels (5–15 %) (Fig. 2**g**), suggesting vacuum-dried aerogels, assisted by a compensation strategy using acrylamide, have an advantage to freeze-dried aerogels in resisting the volume shrinkage.The pristine freeze-dried aerogel shows a volume shrinkage of 20.2 %. However, the volume shrinkage of the vacuum-dried aerogels ranges from 5.3 % to 15.8 % (Fig. S4**f**). The shrinkage of freeze-dried aerogel deteriorates to 50 % as the PEDOT/PSS content reduces and is far higher than the vacuum-dried aerogel counterpart. The increasing water content may account for increased shrinkage due to larger ice crystals extruding slight PEDOT/PSS into weaker 3D structures of aerogel prone to collapse. The low shrinkage is essential for preparing aerogel with a lower density. The minor shrinkage of the vacuum-dried aerogel is probably because the more evenly distributed acrylamide crystals to stabilize the structure to prevent the collapse of the aerogel.

Fig. 2**h** shows the electrical conductivity of the vacuum-dried aerogels compared with the freeze-dried aerogel. Generally, the electrical conductivity of vacuum-dried aerogels (22.9–81.1 S/m) is about three orders of magnitude of the freeze-dried aerogels (0.01–0.02 S/m). This dramatic enhancement in electrical conductivity may be related to the interaction of acrylamide with PEDOT, as suggested in Fig. 1**d**. Another experiment on whether acrylamide acts as a conductivity enhancer for PEDOT/PSS is conducted to understand this improvement. The freeze-dried PEDOT/PSS aerogels are annealed by acrylamide vapor, and the electrical conductivity rises from 0.02 to 29.2 S/m, which is in the same range as vacuum-dried aerogels. This result confirms that acrylamide, as a polar molecule, plays a crucial role in conductivity enhancement through vacuum drying or vapor annealing. Post-treatments like heating, polar solvents immersing, vapor annealing, etc., have improved the conductivity of PEDOT aerogel [35]. This acrylamide-assisted vacuum drying combines the aerogel formation and the post-treatment into one step, reducing the shrinkage while improving the electrical conductivity effectively. Overall, the acrylamide-assisted vacuum drying at 110 °C manages to construct the aerogel with a shorter time, lower shrinkage, and higher conductivity than freeze-drying.

2.3. Electrical conductivity enhancement mechanism of PEDOT/PSS

To confirm the role of acrylamide in enhancing conductivity and further investigate the mechanism, pristine spin-coated PEDOT/PSS and PEDOT/PSS/acrylamide films were vacuum-dried separately at 110 °C to respective electrical conductivities of 4.0 and 1089.3 S/cm. The three orders of magnitude conductivity enhancement agree with the trend in aerogels, as indicated in Fig. 2**h**. The SEM image shows that the pristine PEDOT/PSS film shows a relatively smooth surface (Fig. 3**a**). For the vacuum-dried PEDOT/PSS/acrylamide film, the surface is covered with many self-arranged lines (Fig. 3**b**), which is correlated to the accumulation of PEDOT upon removal acrylamide during vacuum drying. To further understand the phenomenon, atomic force microscope (AFM) associated with a current mode is used to reveal these films' surface characteristics and conduction mechanisms. The height image of the pristine PEDOT/PSS film exhibits nanograin structures and appears relatively smooth with a root-mean-square (RMS) roughness of 1.9 nm. The vacuum-dried PEDOT/PSS/acrylamide film shows non-obvious grain structures but elongated line networks, increasing the RMS roughness to 16.3 nm. Moreover, self-assembled lines with a height of 95.3 nm are observed, which agrees with the lines shown in Fig. 3**b**. The apparent increase in the aspect ratio of PEDOT/PSS grains suggests that acrylamide may function to direct the arrangement of PEDOT, leading to the dramatic enhancement of the electrical conductivity. Corresponding to the AFM height images, their current maps compare the electrical properties from the nanoscale's perspective and represent the distribution of local conductivity in Fig. 3**c and d**. The bright regions indicate the highly conductive domains, and the brown and dark indicate the typical conductive and non-conductive regions. The current mapping of the pristine PEDOT/PSS film displays scattered brown points with a mean current density of 2.8nA/μm^2, suggesting relatively non-conductive characteristics. In contrast, the self-assembled line in vacuum-dried PEDOT/PSS/acrylamide film displays a current density of 17710.9nA/μm^2, strongly related to the PEDOT rich region. The current density near the lines reduces to 653.4nA/μm^2 brought by the less PEDOT away from the PEDOT rich line region. However, it is still higher than the PEDOT/PSS film (2.8nA/μm^2), and the enhancement may ascribe to more PEDOT on the upper layer. The acrylamide redirects the distribution of the PEDOT and leads to the accumulation of the PEDOT on the edge of the crystal. The less PEDOT appears as the particles in other areas (current mapping image in Fig. 3**d**). On the other hand, it forms a conductive network by connecting the PEDOT particles and the rich line region.

The base nature of acrylamide is inclined to combine with acidic PSS in the dispersion to film, proven by UV–vis spectrophotometer, where these films prepared from the above two dispersions are tested before and after vacuum drying. Previous studies commonly reported that the pristine PEDOT/PSS film shows the UV absorption bands located at about 200 and 225 nm, originating from the aromatic ring in PSS [36–38]. In Fig. 3**e**, the PEDOT/PSS film shows 200 and 225 nm UV absorption bands, suggesting no significant change in PSS properties before and after drying. In Fig. 3**f**, the absorption peak at 197 nm is ascribed to the alkene double bond for the pure acrylamide sample. However, for the PEDOT/PSS/acrylamide film, an absorption peak at 254 nm appears and disappears after drying. It is reasonable to understand that acrylamide is removed through vacuum drying and allows the emergence of the absorption bands of the aromatic ring. It is revealed that three absorption peaks originate from the benzene ring except the two mentioned above, and the third one is a weaker band at 254 nm

[39]. They are all strongly related to the substituent group, and the band of 254 nm from PEDOT/PSS film is rarely mentioned in previous studies. This result indicates that the absorption peak at 254 nm is attributed to the existence of acrylamide and might relate to the acid-base effect between a sulfonic acid group of PSS and the primary amine of acrylamide, as shown in the inset image of Fig. 3**f**. An amine group is an electron-donating group due to the inherent lone pair electrons, while the sulfonic acid group is an electron-attracting group leading the peak of 254 nm undetected. However, the acrylamide compensates for the loss of the π-π conjugation of the aromatic ring, and the peak of 254 nm reappears. In summary, acrylamide promotes phase separation of PEDOT and PSS during vacuum drying, facilitating aggregation of PEDOT domains to enhance conductivity.

2.4. Chemical and structure analysis of the aerogels

Fig. 4**a** shows the FTIR spectra of PEDOT/PSS aerogels prepared by freeze-drying and vacuum drying at 80 and 110 °C. The peaks in the FTIR spectra of these three PEDOT/PSS aerogels appear the same, and these two kinds of aerogels show the characteristic peaks of PEDOT/PSS. The peak at 920 cm^{-1} of PEDOT is due to C—S—C vibrations in the thiophene rings, and the peak at 1005 cm^{-1} and 1032 cm^{-1} is due to O—S—O in the sulfonate group from PSS; the peak at 1124 cm^{-1} corresponds to the C—O—C vibrations [40–42]. Compared to the FTIR spectra of acrylamide and polyacrylamide (**Fig. S5**), 1426 cm^{-1} and 1350 cm^{-1} are related to the C—N stretching and N—H scissoring in acrylamide, confirming that no apparent acrylamide or polymerized acrylamide remained in the vacuum-dried aerogels.

Fig. 4**b** presents the Raman spectra of aerogels prepared by freeze-drying and vacuum drying at 80 and 110 °C. The 1265, 1365, and 1426 cm^{-1} peaks of freeze-dried aerogel are attributed to C_α-$C_{\alpha'}$ interring stretching, C_β-C_β stretching, and C_α-C_β stretching in the aromatic thiophene ring of PEDOT [40–42]. The C_α-C_β stretching peak at 1426 cm^{-1} shifts to lower wavenumbers by 14 cm^{-1} and 11 cm^{-1} in vacuum-dried aerogels at 80 and 110 °C, respectively. This change probably correlates to the polar molecule structure and the dipole interaction of acrylamide with PEDOT, resulting in the PEDOT chain structure partially changing from benzoid structure to the most preferred quinoid structure in PEDOT [43], resulting in the conductivity enhancement by acrylamide (Fig. 2**h**).

X-ray diffraction spectra are used to study the structural differences of PEDOT/ PSS (Fig. 4**c**). The lattice spacing (d) is calculated by Bragg's law. The XRD pattern of the freeze-dried aerogel presents two characteristic peaks, the 2θ at 3.4° (d = 25.7 Å) and 25.6° (d = 3.5 Å). The 2θ at 3.4° corresponds to the lamella stacking distance d (1 0 0) of two different ordering distances of the PEDOT and PSS chains [40,44]. The high angle reflection at 25.7° is attributed to the π-π stacking distance d (0 1 0) of PEDOT [44]. At the low angles, 2θ = 3.5° shifts to 3.4° and 3.3° in vacuum-dried aerogel of 80 and 110 °C, respectively, suggesting increased lamella stacking distance d (1 0 0) and a more planar structure from acrylamide-assisted vacuum drying. Whereas the vacuum-dried aerogels display a prominent peak at 26.0°, indicating d (0 1 0) of the π-π stacking distance of the PEDOT reduces from 3.5 to 3.4 Å. Reducing the π-π stacking distance proves the conversion of PEDOT structure from benzoid to quinoid and, therefore, becomes more planar [44].

Though the PEDOT domains are accumulated by acrylamide crystal through phase separation, XPS was used to study surface element valence and the chemical environment (Fig. 4**d**). For PEDOT/PSS, the doublet XPS peaks ($2p_{1/2}$ and $2p_{3/2}$) between 166 and 172 eV are contributed by the S_{2p} band of the sulfur atoms in PSS, while the doublet XPS peaks ($2p_{1/2}$ and $2p_{3/2}$) with binding energies between 162 and 166 eV are contributed by the S_{2p} band of the sulfur atom in the thiophene ring of the PEDOT [45]. The relative intensity of PSS is calibrated to the same level to compare the surface information of the freeze-dried and vacuum-dried aerogels. The PEDOT-to-PSS ratio (R_s) is determined by quantitative analysis of the S_{2p} core-level spectra. Compared with freeze-dried aerogels (R_s = 0.46), the vacuum-dried aerogels present higher R_s of 0.84 at 80 and 110 °C, respectively. These results suggest that the PEDOT is rich, and the separated PEDOT domains are spread on the film's surface. This is believed that the acrylamide crystal ascribes the conductivity enhancement of the vacuum-dried aerogels for promoting the conversion of PEDOT structure from benzoid to quinoid and accumulating the PEDOT domains on the surface of PSS (Fig. 4**d**). Fig. 4**e** shows a schematic microstructure change of the PEDOT/PSS aerogel via the acrylamide-assisted vacuum drying as manifested by the chemical and structural analysis results. The acrylamide plays a crucial role in PEDOT/PSS aerogel formation throughout the vacuum drying, while its polar molecule structure also induces dipole–dipole interaction with thiophene rings in PEDOT [46]. Though it is beyond the scope of this study to quantify the ratio between the quinoid and benzoid structures in the aerogel, we could still remark that a more favorable quinoid structure leads to planarization of the conductive PEDOT chains, resulting in the reduction of π-π stacking distance to reduce the electron pathways on the chains and increase conductivity of the aerogel.

3. Universality of the approach and the application of aerogels as electric generators

Our acrylamide-assisted vacuum drying approach shows a certain universality applied in different material systems. Besides conductive polymers, the reliability of the approach is explored on different nanomaterials, such as cellulose nanofibers (CNFs) and multi-walled carbon nanotubes (MWCNTs), which are the typical representatives of biopolymers and carbon nanomaterials [9,47,48]. When forming aerogels, a relatively strong polymer is necessary to serve as the main structure to resist surface tension and capillary pressure.

As far as the CNF aerogel is concerned, alginate is used to realize a crosslinked structure to reinforce the aerogels [17]. With the acrylamide involved, the CNFs/alginate gel is moved to the vacuum oven after being frozen, and the CNFs/alginate aerogel with a density of 84.1 mg/cm^3 is obtained, as shown in the inset of Fig. 5**a** (see more experiment details in the supporting information). The SEM image of the CNFs/alginate aerogel reveals a laminar structure and micrometer pores inside (Fig. 5**a**). Inspired by a combination of PEDOT and PSS, we assume that the formation of MWCNT aerogel can be realized by using a polymer as the backbone in acrylamide-assisted vacuum drying. Here, carboxymethyl chitosan is chosen because it is known for its capability to form gels [49]. The acrylamide with a specific weight ratio is added to form MWCNTs/carboxymethyl chitosan gel, followed by freezing and vacuum drying. The inset of Fig. 5**b** displays the MWCNTs/carboxymethyl chitosan aerogel prepared by this method with a density of 87.4 mg/ cm^3. The micrometer pores are uniformly distributed inside the MWCNTs/carboxymethyl chitosan aerogel (Fig. 5**b**). Thus, the universality of the approach is proved by the successful processing of conductive polymers, biopolymers, and carbon nanomaterials aerogels by introducing acrylamide as the assisting solute.

The highly porous nature and high surface area enable these aerogels to contact water to a large extent. The hydrophilic groups like –OH and –COOH endow them to be used as water-induced electric generators for collecting green energy [50–52]. To investigate the generating efficiency of water-induced electric generators, these three kinds of aerogels are chosen as the representative material for functional polymer, biomass material and nanocarbon material. Fig. 5**c** shows the experimental set-up of the water-induced electric generator where PEDOT/PSS aerogel. CNF/alginate aerogel, and MWCNTs/carboxymethyl chitosan aerogel are used as the water transporting media. The critical working mechanism lies in the ionic concentration difference between the bottom and top sides of the aerogel, which is necessary for activating electrical potential difference of the generator [50,52]. As for water-induced electrical generators, PEDOT/PSS/graphene oxide composite aerogels have been studied previously, but pristine PEDOT/PSS aerogels have not been analyzed yet [50]. Higher conductivity of PEDOT/PSS is

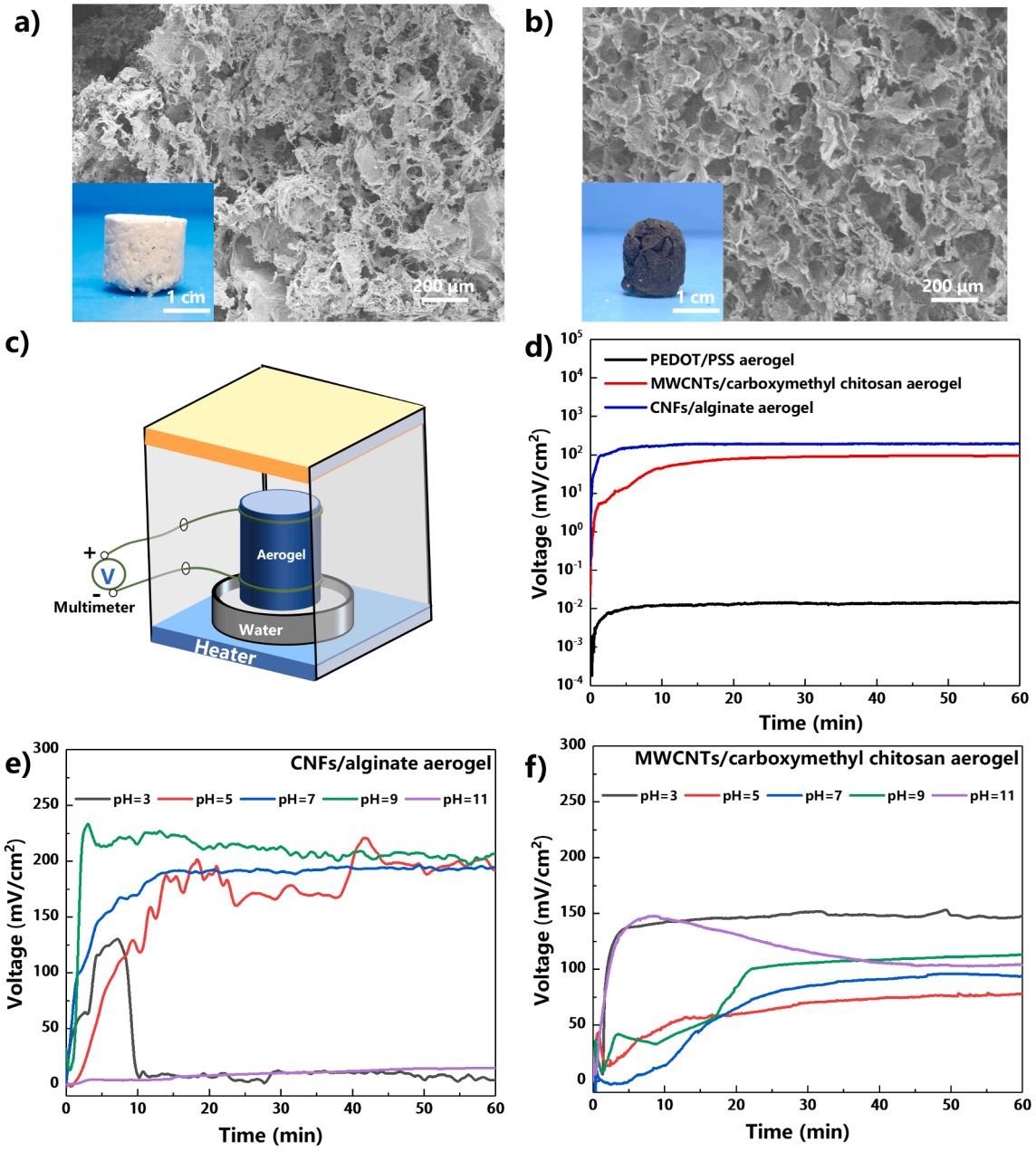

Fig. 5. The universality of acrylamide-assisted vacuum drying and the application of aerogel as electric generators. a) The SEM image of CNFs/alginate aerogel and its digital picture (the inset). b) The SEM image of MWCNTs/carboxymethyl chitosan aerogel and its digital picture (the inset). c) The experimental set-up of the water-induced electric generator. d) The generated voltage of the water-induced electric generator using PEDOT/PSS aerogel, CNFs/alginate aerogel, and MWCNTs/carboxymethyl chitosan aerogel. e) The generated voltage of CNFs/alginate aerogels in different pH solutions. The generated voltage remains around 200 mV/cm^2 between pH = 5–9 and decreases sharply in pH = 3 and pH = 11. f) The generated voltage of MWCNTs/carboxymethyl chitosan aerogel in different pH solutions. The generated voltage remains around 90 mV/cm^2 between pH = 5–9 and increases in pH = 3 and pH = 11.

obtained via acrylamide-assisted vacuum drying and higher conductivity means the lower internal resistance of the water-induced electrical generators. Moreover, uneven water distribution is a good candidate for causing ionic concentrations. Water from the solution could be easily absorbed into the highly porous structures based on their capillary pressure due to the presence of extensive hydrophilic groups in the aerogels. For instance, the sulfonic acid group of PSS in PEDOT/PSS aerogels, the carboxyl and hydroxyl groups in CNF/alginate aerogels, and MWCNTs/carboxymethyl chitosan aerogels. The absorbed water from the solution forms a water layer on the cellular walls of the aerogels, helping the protons (H^+) to migrate from the sulfonic acid, hydroxyl, and carboxyl groups. Thus, the ionic pathways can be generated due to water absorption and the induced ionic concentration difference from the bottom to the surface of the aerogel. Fig. 5**d** shows a preliminary experiment result for these aerogels to generate energy. The generated voltage from PEDOT/PSS aerogel is 0.03 mV/cm^2 at ambient temperature, while CNF/alginate aerogel and MWCNTs/carboxymethyl chitosan aerogel display steady voltages of 87.3 and 195.0 mV/cm^2 after 5 to 10 mins, respectively.

To improve the energy generation performance of these aerogels, a temperature difference (ΔT) from the bottom to the top surface of PEDOT/PSS aerogel is conducted by heating water (the insert of Fig. S7**a**). This allows us to use the thermoelectric effect of the PEDOT/PSS [36,38]. PEDOT/PSS aerogel, as a thermoelectric material, can harvest higher voltage in larger temperature gap. This temperature gap induces quick transportation of water micro-droplets and leads to higher

evaporation rate, so redistribution of the surface charge happens. Fig. S7**a** collects the voltage in different ΔT, which is positively associated with the generated voltages. When the ΔT is equal to 0 °C, the water is unheated, and only a small voltage of 0.03 mV/cm^2 is detected. When the ΔT rises to 10, 20, 30, and 40 °C, the voltage reaches 5.1, 12.5, 34.8, and 68.2 mV/cm^2, respectively. Further improvement of generated voltages in CNFs/alginate aerogels and MWCNTs/carboxymethyl chitosan aerogels can be obtained by tuning the pH values of the solution. The functional groups of CNFs/alginate and carboxymethyl chitosan are mainly –OH and –COOH enabling the absorption of H^+ and OH^-, increasing the ion concentration between the near-water side and the away-water side. For CNFs/alginate aerogels, the generated voltage remains about 200 mV/cm^2 when the solution pH values stay between 5 and 9. However, an apparent decrease was observed at pH values of 3 and 11, where the generators only provide about 11 mV/cm^2 voltage (Fig. 5**e**). These results suggest that the destruction of the aerogel structure is probably brought by the high ion concentration of H^+ and OH^-, accounts for the decrease.

On the contrary, the MWCNTs/carboxymethyl chitosan aerogels present higher voltages of 148.9 and 112.0 mV/cm^2 at pH 3 and 11, respectively (Fig. 5**f**). In contrast, the high H^+ and OH^- concentrations bring higher voltage because the structure of the MWCNTs/carboxymethyl chitosan aerogels can remain intact in either acid or alkali environment. Moreover, due to the reinforced crosslinked structure of carboxymethyl chitosan, the wet-stability of MWCNTs/carboxymethyl chitosan aerogels is superior to those of PEDOT/PSS and CNFs/alginate aerogels, where the later two collapse and fail to maintain the structure after re-drying. Thus, we define a cyclic wetting and drying process to verify the reusability and wet-stability of the MWCNTs/carboxymethyl chitosan aerogels. Fig. S7**b** shows the generated voltage after 10, 50, and 100 cyclic wetting and drying process. They all maintain a voltage around 90 mV/cm^2, proving excellent wet-stability of MWCNTs/carboxymethyl chitosan aerogels.

4. Conclusion

The novel acrylamide-assisted vacuum drying approach has been validated and demonstrated for efficient construction of PEDOT/PSS aerogels, and its underlying mechanism is systematically studied. Without any specific device such as lyophilizers or supercritical driers, acrylamide-assisted vacuum drying is not only simple, highly efficient, energy-conserving, and time saving, but also only requires an ordinary vacuum oven and eliminates the overuse of organic solvents as in ambient drying method. Meanwhile, it presents a possibility in the recycling of acrylamide. The aerogels prepared at 110 °C exhibits a density as low as 6.3 mg/cm^3 with an electrical conductivity of 81.1 S/m, which is improved by three orders of magnitude compared to the freeze-dried aerogel without any post-treatment. Besides, the shrinkage of the vacuum-dried aerogel is from 5 to 15 %, lower than 20 % of freeze-dried aerogel even when the PEDOT/PSS content is equal. Acrylamide in this approach acts to significantly reduce the surface tension and capillary pressure to retain the lamellar structure during vacuum drying. Moreover, the acrylamide prompts the phase separation of PEDOT and PSS, leading to the concentrated PEDOT domains inside the aerogels and converting PEDOT's benzoid structure to quinoid structure, both contributing to the enhancement of conductivity. Additionally, universality of the acrylamide-assisted vacuum drying approach is proved by realizing CNF/alginate aerogels and MWCNTs/carboxymethyl chitosan aerogels. The ultra-porous and wet resilient aerogel structure favors the mobility of water molecules and provides a steady voltage as the water-induced electric generators. The compensation strategy using acrylamide-assisted vacuum drying can be generalized for an expansive material library and provides an alternative way for customized aerogel preparation with designed functionality, thus making aerogels applicable for their target uses.

5. Experimental section

Materials: Acrylamide (>99.8 wt% purity) was purchased from Sigma-Aldrich. Aqueous poly(3,4-ethylene dioxythiophene)/poly(styrene sulfonate) (PEDOT/PSS, Clevios pH 1000) dispersion with a concentration of 1.1 wt% and PEDOT to PSS weight ratio of 1 to 2.5 was purchased from Heraeus, Inc.

Investigation of temperature window of the acrylamide for aerogel formation: Weighed acrylamide was placed on a glass petri dish and vacuum dried at different temperatures (20, 35, 50, 65, 80, 95, 110, and 140 °C) for 6 h to measure the mass and the residual ratio of acrylamide at each temperature was obtained.

Preparation of vacuum-dried and freeze-dried PEDOT/PSS aerogels: Acrylamide was mixed with pristine PEDOT/PSS aqueous dispersion at various dispersion-to-acrylamide weight ratios (1:x, x = 0.5, 0.75, 1.00, 1.25, 1.5), as shown in Table S1. The PEDOT/PSS/acrylamide mixtures were stirred for 12 h, loaded into the drying molds (Fig. S2**b**) and frozen at −18 °C for 12 h, then dried in a vacuum oven (YiHeng, Inc, DZF-6050) at 50 °C, 80 °C, and 110 °C for 6 h to obtain the aerogels. The freeze-dried aerogels were prepared by freeze-drying PEDOT/PSS aqueous dispersion with the same weight ratio of water as acrylamide to ensure the same PEDOT/PSS contents, then frozen (-18 °C, 12 h) and freeze-dried (-50 °C, 48 h, BIOCOOL Inc., FD-1A-50) for comparison. To prove the conductivity enhancement effect of acrylamide vapor annealing, the freeze-dried PEDOT/PSS (using 1.1 wt% aqueous PEDOT/PSS dispersion) aerogels and 10 g acrylamide were placed in a close glass jar at 110 °C for 6 h.

Calculation of the porosity and shrinkage of the aerogels: The porosity (P) of PEDOT/PSS aerogel was calculated as, $P = (\rho_0-\rho) / \rho_0 \times 100$ %, where ρ_0 is the density of PEDOT/PSS solid (1.15 g/cm^3) and ρ the is the density of aerogel [53]. The shrinkage was calculated by $(1- V/V_o) \times 100$ %, where V_o is the volume of the frozen solid, and V is the volume of the aerogel.

Preparation of PEDOT/PSS/acrylamide and pristine PEDOT/PSS films: Aqueous PEDOT/PSS/acrylamide mixture was prepared at 1:0.75 dispersion-to-acrylamide ratio and the pristine PEDOT/PSS aqueous dispersion was mixed with water at the same quantity as acrylamide (see details on Table S1). These dispersions were spin-coated on the O_2 plasma-treated hydrophilic glass substrates at 1000 rpm for 25 s. Then the films were vacuum-dried at 110 °C for 6 h.

Construction of the water-induced electric generators: aerogels were cut into cuboid pieces (0.8 × 2 cm^2) and two ends were pasted with the conductive epoxy (Chemtronics, CW2400). Then each side was connected with a copper wire electrode. After oven (45 °C) drying for 3 h, the device was hung overhead a dish filled with deionized water before immersing the end in the water. As one end contacted the water downward, the voltage data was starting to be collected by a multimeter.

Characterization: The surface tension of aqueous PEDOT/PSS/acrylamide dispersion was recorded by a drop shape analyzer (DSA100B, KRUSS). The electrical conductivity of freeze-dried and vacuum-dried PEDOT/PSS aerogels was calculated using $\sigma = L / (R \cdot S)$, where L is the length, R is the resistance, and S is the cross-section area of the aerogel. To measure the R, two ends of the aerogel were pasted with the conductive epoxy (Chemtronics, CW2400) and each side was connected to a copper wire electrode. Then R was measured with a multimeter. Sheet resistance of the spin-costing film was measured by the 4-point probe method (3-M, Jingge). The thickness of the film was recorded using a profilometer (Bruker Dektak XT stylus) and the electrical conductivity (σ) was calculated as, $\sigma = 1 / (R_s \cdot t)$, where R_s is the sheet resistance and t is the thickness. Cold-field-emission scanning electron microscopy (SEM, Hitachi, SU8010,10 kV) was used to study the morphology of the vacuum dried and freeze-dried PEDOT/PSS aerogels. The microscopic surface morphology and current mapping measurements were conducted on Bruker icon Dimension with scan Asyst atomic force microscopy (AFM). For conductive AFM, the samples were spin-coated on the ITO substrate (O_2 plasma-treated) at 1000 rpm for 25 s,

and the PFTUNA probes were used to obtain the map topography and current under the bias of 50 mV for PEDOT/PSS/acrylamide films and 1200 mV for PEDOT/PSS films. The UV absorption of films was conducted by a UV–vis-NIR spectrometer (PerkinElmer, Lamdba 950). The 1:0.75 aerogels were characterized as follows. Fourier transform infrared spectra (FTIR) (TENSOR 27, Bruker) of the freeze-dried and vacuum-dried aerogels were investigated in the Attenuated Total Reflection (ATR) mode at a resolution of 4 cm^{-1}. Raman spectra were obtained by an RM1000 Raman spectrometer (inVia Reflex, Renishaw) on aerogels using a 633 nm argon-ion laser. The X-ray diffraction (XRD) was measured in a Bruker Rigaku Smartlab diffractometer equipped with a Cu Kα source (λ = 1.54178 Å). XPS (Thermo Fisher Scientific, Nexsa) spectra were collected using monochromatic, micro-focused (spot size = 400 μm) Al Ka X-ray photons (hν = 1486.6 eV) at a base pressure of 10–9 Torr.

Declaration of Competing Interest

The authors declare that they have no known competing financial interests or personal relationships that could have appeared to influence the work reported in this paper.

Data availability

Data will be made available on request.

Acknowledgments

The Natural Science Foundation of Guangdong Province (2019A1515011812), the 100 Top Talents Program-Sun Yat-sen University (29000-18841225), and Fundamental Research Funds for the Central Universities (20lgpy12) is gratefully acknowledged. Thanks for the research fund from Guangzhou Key Laboratory of Flexible Electronic Materials and Wearable Devices.

Appendix A. Supplementary data

Supplementary data to this article can be found online at https://doi.org/10.1016/j.cej.2022.139685.

References

[1] S. Tang, X. Zhang, J. Fan, B. Li, Z. Li, C. Wang, H. Li, P. Zhang, J. Zhou, Fibrillation of well-formed conductive aerogel for soft conductors, Appl. Mater. Today 26 (2022), 101399.
[2] N. Hüsing, U. Schubert, Aerogels—airy materials: chemistry, structure, and properties, Angew. Chem. Int. Ed. 37 (1–2) (1998) 22–45.
[3] A.C. Pierre, G.M. Pajonk, Chemistry of aerogels and their applications, Chem. Rev. 102 (11) (2002) 4243–4265, https://doi.org/10.1021/cr0101306.
[4] A.S. Dorcheh, M.H. Abbasi, Silica aerogel; synthesis, properties and characterization, J. Mater. Process. Technol. 199 (1–3) (2008) 10–26, https://doi.org/10.1016/j.jmatprotec.2007.10.060.
[5] R. Baetens, B.P. Jelle, A. Gustavsen, Aerogel insulation for building applications: A state-of-the-art review, Energy Build. 43 (4) (2011) 761–769, https://doi.org/10.1016/j.enbuild.2010.12.012.
[6] M.J. Burchell, G. Graham, A. Kearsley, Cosmic dust collection in aerogel, Annu. Rev. Earth Planet. Sci. 34 (2006) 385–418, https://doi.org/10.1146/annurev.earth.34.031405.124939.
[7] Z. Chen, H. Zhuo, Y. Hu, H. Lai, L. Liu, L. Zhong, X. Peng, Wood-derived lightweight and elastic carbon aerogel for pressure sensing and energy storage, Adv. Funct. Mater. 30 (17) (2020) 1910292.
[8] Z. Mazrouei-Sebdani, H. Begum, S. Schoenwald, K.V. Horoshenkov, W.J. Malfait, A review on silica aerogel-based materials for acoustic applications, J. Non-Cryst. Solids 562 (2021), 120770.
[9] C. Moreno-Castilla, F. Maldonado-Hódar, Carbon aerogels for catalysis applications: An overview, Carbon 43 (3) (2005) 455–465.
[10] P. Min, X. Li, P. Liu, J. Liu, X.Q. Jia, X.P. Li, Z.Z. Yu, Rational design of soft yet elastic lamellar graphene aerogels via bidirectional freezing for ultrasensitive pressure and bending sensors, Adv. Funct. Mater. 31 (34) (2021) 2103703.
[11] X.-J. Yu, J. Qu, Z. Yuan, P. Min, S.-M. Hao, Z.-S. Zhu, X. Li, D. Yang, Z.-Z. Yu, Anisotropic CoFe2O4@ graphene hybrid aerogels with high flux and excellent stability as building blocks for rapid catalytic degradation of organic contaminants in a flow-type setup, ACS Appl. Mater. Interfaces 11 (37) (2019) 34222–34231.
[12] C.A. García-González, M.C. Camino-Rey, M. Alnaief, C. Zetzl, I. Smirnova, Supercritical drying of aerogels using CO2: Effect of extraction time on the end material textural properties, J. Supercrit. Fluids 66 (2012) 297–306, https://doi.org/10.1016/j.supflu.2012.02.026.
[13] X. Han, K.T. Hassan, A. Harvey, D. Kulijer, A. Oila, M.R.C. Hunt, L. Siller, Bioinspired Synthesis of Monolithic and Layered Aerogels, Adv. Mater. 30 (23) (2018) e1706294.
[14] Z. Ulker, C. Erkey, An emerging platform for drug delivery: Aerogel based systems, J. Control. Release 177 (2014) 51–63, https://doi.org/10.1016/j.jconrel.2013.12.033.
[15] H. Namatsu, K. Yamazaki, K. Kurihara, Supercritical drying for nanostructure fabrication without pattern collapse, Microelectron. Eng. 46 (1–4) (1999) 129–132.
[16] S. Tang, M. Ma, X. Zhang, X. Zhao, J. Fan, P. Zhu, K. Shi, J. Zhou, Covalent crosslinks enable the formation of ambient-dried biomass aerogels through the activation of a triazine derivative for energy storage and generation, Adv. Funct. Mater. 32 (36) (2022) 2205417, https://doi.org/10.1002/adfm.202205417.
[17] H. Françon, Z. Wang, A. Marais, K. Mystek, A. Piper, H. Granberg, A. Malti, P. Gatenholm, P.A. Larsson, L. Wågberg, Ambient-Dried, 3D-Printable and Electrically Conducting Cellulose Nanofiber Aerogels by Inclusion of Functional Polymers, Adv. Funct. Mater. 30 (12) (2020) 1909383.
[18] Y. Lin, F. Liu, G. Casano, R. Bhavsar, I.A. Kinloch, B. Derby, Pristine Graphene Aerogels by Room-Temperature Freeze Gelation, Adv. Mater. 28 (36) (2016) 7993–8000, https://doi.org/10.1002/adma.201602393.
[19] J. Rostami, K. Gordeyeva, T. Benselfelt, E. Lahchaichi, S.A. Hall, A.V. Riazanova, P. A. Larsson, G. Cinar Ciftci, L. Wågberg, Hierarchical build-up of bio-based nanofibrous materials with tunable metal–organic framework biofunctionality, Mater. Today 48 (2021) 47–58, https://doi.org/10.1016/j.mattod.2021.04.013.
[20] K. Sun, P. Li, Y. Xia, J. Chang, J. Ouyang, Transparent conductive oxide-free perovskite solar cells with PEDOT:PSS as transparent electrode, ACS Appl. Mater. Interfaces 7 (28) (2015) 15314–15320, https://doi.org/10.1021/acsami.5b03171.
[21] X. Fan, W. Nie, H. Tsai, N. Wang, H. Huang, Y. Cheng, R. Wen, L. Ma, F. Yan, Y. Xia, PEDOT:PSS for Flexible and Stretchable Electronics: Modifications, Strategies, and Applications, Adv Sci (Weinh) 6 (19) (2019) 1900813, https://doi.org/10.1002/advs.201900813.
[22] Z. Fan, P. Li, D. Du, J. Ouyang, Significantly Enhanced Thermoelectric Properties of PEDOT:PSS Films through Sequential Post-Treatments with Common Acids and Bases, Adv. Energy Mater. 7 (8) (2017) 1602116, https://doi.org/10.1002/aenm.201602116.
[23] S. Han, N.U.H. Alvi, L. Granlof, H. Granberg, M. Berggren, S. Fabiano, X. Crispin, A Multiparameter Pressure-Temperature-Humidity Sensor Based on Mixed Ionic-Electronic Cellulose Aerogels, Adv Sci (Weinh) 6 (8) (2019) 1802128, https://doi.org/10.1002/advs.201802128.
[24] B. Yang, F. Yao, L. Ye, T. Hao, Y. Zhang, L. Zhang, D. Dong, W. Fang, Y. Wang, X. Zhang, C. Wang, J. Li, A conductive PEDOT/alginate porous scaffold as a platform to modulate the biological behaviors of brown adipose-derived stem cells, Biomater. Sci. 8 (11) (2020) 3173–3185, https://doi.org/10.1039/c9bm02012h.
[25] T.A. Jennings, Lyophilization: introduction and basic principles, CRC press1999.
[26] G. Nireesha, L. Divya, C. Sowmya, N. Venkateshan, V. Lavakumar, Lyophilization/freeze drying-an review, Int. Novel Trends Pharmaceut. Sci. 3 (4) (2013) 87–98.
[27] J.P. Fouassier, D.J. Lougnot, I. Zuchowicz, P.N. Green, H.J. Timpe, K.P. Kronfeld, U. Müller, Photoinitiation mechanism of acrylamide polymerization in the presence of water-soluble benzophenones, Journal of Photochemistry 36 (3) (1987) 347–363, https://doi.org/10.1016/0047-2670(87)80025-4.
[28] S.-Y. Huang, D.W. Lipp, R.S. Farinato, Acrylamide Polymers, Kirk-Othmer Encyclopedia of Chemical Technology. doi: 10.1002/0471238961.0103182512091616.a01.pub2.
[29] T.A. Fadner, H. Morawetz, Polymerization in the crystalline state. I. Acrylamide, Journal of Polymer Science 45(146) (1960) 475–501, https://doi.org/10.1002/pol.1960.1204514617.
[30] K.B. Girma, V. Lorenz, S. Blaurock, F.T. Edelmann, Coordination chemistry of acrylamide, Coord. Chem. Rev. 249 (11–12) (2005) 1283–1293, https://doi.org/10.1016/j.ccr.2005.01.028.
[31] A.A. Udovenko, L.G. Kolzunova, Crystal structure of acrylamide, J. Struct. Chem. 49 (5) (2008) 961–964, https://doi.org/10.1007/s10947-008-0165-6.
[32] O.L. Brown, The Clausius-Clapeyron equation, J. Chem. Educ. 28 (8) (1951) 428.
[33] J. Kołaczkiewicz, E. Bauer, Clausius-Clapeyron equation analysis of two-dimensional vaporization, Surf. Sci. 155 (2–3) (1985) 700–714.
[34] J.-H. Zhu, F. Shao, Y.-H. Zhan, X.-L. Yan, B. Zhang, Acrylamide as cosurfactant and hydrotrope in the pseudoternary Span 80-Tween 85/isopar M/water emulsion/microemulsion forming system, Colloids Surf., A 290 (1) (2006) 19–24, https://doi.org/10.1016/j.colsurfa.2006.04.044.
[35] H. Shi, C. Liu, Q. Jiang, J. Xu, Effective approaches to improve the electrical conductivity of PEDOT: PSS: a review, Adv. Electron. Mater. 1 (4) (2015) 1500017.
[36] Z. Fan, P. Li, D. Du, J. Ouyang, Significantly enhanced thermoelectric properties of PEDOT: PSS films through sequential post-treatments with common acids and bases, Adv. Energy Mater. 7 (8) (2017) 1602116.
[37] Y. Xia, J. Ouyang, Anion effect on salt-induced conductivity enhancement of poly (3, 4-ethylenedioxythiophene): poly (styrenesulfonate) films, Org. Electron. 11 (6) (2010) 1129–1135.
[38] S. Zhang, Z. Fan, X. Wang, Z. Zhang, J. Ouyang, Enhancement of the thermoelectric properties of PEDOT:PSS via one-step treatment with cosolvents or their solutions of organic salts, J. Mater. Chem. A 6 (16) (2018) 7080–7087, https://doi.org/10.1039/C7TA11148G.
[39] N. Brennan, UV/VIS Spectroscopy, University of Pretoria, etd (2006) 109-121.

[40] B. Li, J. Li, D. Ni, S. Tang, J. Fan, K. Shi, Z. Li, J. Zhou, Spontaneously spread polymer thin films on the miscible liquid substrates, Chem. Eng. J. 437 (2022), 135443.
[41] B. Li, D. Ni, J. Fan, J. Zhou, Vapor phase polymerized high-performance Poly(3,4-ethylenedioxythiophene) using polyethyleneimine (PEI) as the base inhibitor and grafting agent for electrochromic medical face shields, Chem. Eng. J. 445 (2022), 136818, https://doi.org/10.1016/j.cej.2022.136818.
[42] J. Zhou, D.H. Anjum, G. Lubineau, E.Q. Li, S.T. Thoroddsen, Unraveling the Order and Disorder in Poly(3,4-ethylenedioxythiophene)/Poly(styrenesulfonate) Nanofilms, Macromolecules 48 (16) (2015) 5688–5696, https://doi.org/10.1021/acs.macromol.5b00851.
[43] S.H. Chang, C.-H. Chiang, F.-S. Kao, C.-L. Tien, C.-G. Wu, Unraveling the enhanced electrical conductivity of PEDOT: PSS thin films for ITO-free organic photovoltaics, IEEE Photonics J. 6 (4) (2014) 1–7.
[44] X. Wang, A.K.K. Kyaw, C. Yin, F. Wang, Q. Zhu, T. Tang, P.I. Yee, J. Xu, Enhancement of thermoelectric performance of PEDOT: PSS films by post-treatment with a superacid, RSC Adv. 8 (33) (2018) 18334–18340.
[45] K. Xing, M. Fahlman, X. Chen, O. Inganäs, W. Salaneck, The electronic structure of poly (3, 4-ethylene-dioxythiophene): studied by XPS and UPS, Synth. Met. 89 (3) (1997) 161–165.
[46] Y. Yang, H. Deng, Q. Fu, Recent progress on PEDOT:PSS based polymer blends and composites for flexible electronics and thermoelectric devices, Mater. Chem. Front. 4 (11) (2020) 3130–3152, https://doi.org/10.1039/d0qm00308e.
[47] J. Zhou, Y.-L. Hsieh, Nanocellulose aerogel-based porous coaxial fibers for thermal insulation, Nano Energy 68 (2020), 104305.
[48] J. Yang, E. Zhang, X. Li, Y. Zhang, J. Qu, Z.-Z. Yu, Cellulose/graphene aerogel supported phase change composites with high thermal conductivity and good shape stability for thermal energy storage, Carbon 98 (2016) 50–57.
[49] Z. Shariatinia, Carboxymethyl chitosan: Properties and biomedical applications, Int. J. Biol. Macromol. 120 (Pt B) (2018) 1406–1419, https://doi.org/10.1016/j.ijbiomac.2018.09.131.
[50] X. Qi, T. Miao, C. Chi, G. Zhang, C. Zhang, Y. Du, M. An, W.-G. Ma, X. Zhang, Ultralight PEDOT:PSS/graphene oxide composite aerogel sponges for electric power harvesting from thermal fluctuations and moist environment, Nano Energy 77 (2020), 105096, https://doi.org/10.1016/j.nanoen.2020.105096.
[51] P. Shukla, P. Saxena, N. Bhardwaj, V.K. Jain, Microporous polymer membrane assisted water induced electricity generation based on triboelectrification and electrostatic induction, RSC Adv. 10 (67) (2020) 40608–40618, https://doi.org/10.1039/d0ra07982k.
[52] Z. Sun, L. Feng, X. Wen, L. Wang, X. Qin, J. Yu, Ceramic Nanofiber-Based Water-Induced Electric Generator, ACS Appl. Mater. Interfaces 13 (47) (2021) 56226–56232, https://doi.org/10.1021/acsami.1c17847.
[53] C. Xie, S. Liu, Q. Zhang, H. Ma, S. Yang, Z.-X. Guo, T. Qiu, X. Tuo, Macroscopic-Scale Preparation of Aramid Nanofiber Aerogel by Modified Freezing-Drying Method, ACS Nano 15 (6) (2021) 10000–10009.